



Universiteit
Leiden
The Netherlands

The fight for a reactive site

Groot, I.M.N.

Citation

Groot, I. M. N. (2009, December 10). *The fight for a reactive site*. Retrieved from <https://hdl.handle.net/1887/14503>

Version: Corrected Publisher's Version

License: [Licence agreement concerning inclusion of doctoral thesis in the Institutional Repository of the University of Leiden](#)

Downloaded from: <https://hdl.handle.net/1887/14503>

Note: To cite this publication please use the final published version (if applicable).

Chapter 3

Calculational methods and approximations

3.1 The Born-Oppenheimer approximation

Central to the modern approach of describing chemical reactivity as dynamics on a potential energy surface is the Born-Oppenheimer approximation [1]. According to this approximation the motion of the electrons re-adjusts instantaneously as heavy nuclei progress through chemical rearrangement, and the nuclear and electronic motion can be decoupled. The use of this approximation stems from the large difference in time-scales for electron motion compared to nuclear motion. For hydrogen dissociation on Pt(111) it was shown that use of the Born-Oppenheimer approximation is justified [2].

The Hamiltonian operator describing the motion of the nuclei and the electrons is given by

$$\hat{H}_{tot}(q_\alpha, q_i) = \hat{K}_n(q_\alpha) + \hat{K}_e(q_i) + \hat{V}_{nn}(q_\alpha) + \hat{V}_{ee}(q_i) + \hat{V}_{ne}(q_\alpha, q_i). \quad (3.1)$$

Here $\hat{K}_n(q_\alpha)$ and $\hat{K}_e(q_i)$ are the kinetic energy operators associated with the nuclei and electrons, respectively; $\hat{V}_{nn}(q_\alpha)$ and $\hat{V}_{ee}(q_i)$ are the potential energy operators associated with the repulsion between the nuclei and the electrons, respectively; and $\hat{V}_{ne}(q_\alpha, q_i)$ is the potential energy operator that describes the attraction between the nuclei and the electrons. q_α and q_i describe the nuclear and electronic coordinates, respectively.

To calculate the total energy of the system, the Schrödinger equation needs to be solved:

$$\hat{H}_{tot}\Psi(q_\alpha, q_i) = E_{tot}\Psi(q_\alpha, q_i), \quad (3.2)$$

where Ψ is the total wave function of the system. The total wave function can be divided in a part describing the nuclei and a part describing the electrons (which interact with the nuclei, hence the occurrence of q_α in Ψ_e in Eq. 3.3):

$$\Psi(q_\alpha, q_i) = \Psi_n(q_\alpha)\Psi_e(q_\alpha, q_i). \quad (3.3)$$

In the same way we will divide the total Hamiltonian in a part describing the nuclei and a part describing the electrons. Equation 3.1 can then be written as:

$$\hat{H}_{tot} = \hat{H}_e + \hat{H}_n(q_\alpha). \quad (3.4)$$

Here the electronic Hamiltonian is given by:

$$\hat{H}_e(q_\alpha, q_i) = \hat{K}_e(q_i) + \hat{V}_{ee}(q_i) + \hat{V}_{nn}(q_\alpha) + \hat{V}_{ne}(q_\alpha, q_i). \quad (3.5)$$

Assuming the following equations to represent good approximations, we introduce the Born-Oppenheimer approximation:

$$\begin{aligned} \frac{\delta}{\delta q_\alpha} \Psi_e(q_\alpha, q_i) &= 0 \\ \frac{\delta^2}{\delta q_\alpha^2} \Psi_e(q_\alpha, q_i) &= 0. \end{aligned} \quad (3.6)$$

The Schrödinger equation for the electronic motion is then written as:

$$\hat{H}_e(q_\alpha, q_i) \Psi(q_\alpha; q_i) = E_e(q_\alpha) \Psi(q_\alpha; q_i), \quad (3.7)$$

where $E_e(q_\alpha)$ is the electronic energy, including internuclear repulsion. The function $E_e(q_\alpha)$ represents the potential energy surface that determines the motion of the nuclei.

3.2 Density functional theory

To calculate the potential energy for the different configurations of H_2 on the surface, density functional theory (DFT) is used. DFT is based on the discovery of Hohenberg and Kohn that for a non-degenerate ground state system of N interacting electrons in an external potential, the ground state energy is uniquely determined by a functional of the electron density [3]. In combination with the use of the Hohenberg-Kohn variational principle [3], Kohn and Sham formulated the many-electron problem (see Eq. 3.5) in terms of single-electron equations [4]:

$$\left[-\frac{1}{2} \nabla^2 + v(q) + \int \frac{\rho(q')}{|q - q'|} dq' + v_{xc}(q) \right] \varphi_i(q) = \epsilon_i \varphi_i(q). \quad (3.8)$$

Here q and q' are electron position vectors, $-\frac{1}{2} \nabla^2$ is the kinetic energy operator, $v(q)$ is the external potential determined by the positions of the nuclei, $\varphi_i(q)$ is the one-electron wave function of electron i , ϵ_i is the one-electron energy, and $\rho(q)$ is the electron density. In Eq. 3.8 and below atomic units are used. The exchange-correlation potential, v_{xc} , is given by

$$v_{xc}(q) = \frac{\delta E_{xc}[\rho(q)]}{\delta \rho(q)}, \quad (3.9)$$

where E_{xc} is the exchange-correlation energy. The electron density is given by

$$\rho(q) = \sum_i^N |\varphi_i(q)|^2. \quad (3.10)$$

If the exchange-correlation function were known exactly, the exact potential energy could be calculated by

$$E_e(q_\alpha) = \sum_i^N \epsilon_i - \frac{1}{2} \int \frac{\rho(q)\rho(q')}{|q-q'|} dqdq' + E_{xc}[\rho] - \int v_{xc}(q)\rho(q) dq + V_{nn}(q_\alpha), \quad (3.11)$$

where $V_{nn}(q_\alpha)$ is the nuclear-nuclear repulsion term as described in Section 3.1. Unfortunately, the exact exchange-correlation functional is not known yet. To approximate the exchange-correlation energy the generalized gradient approximation (GGA) will be used in the work described in Chapters 5 and 6. In the GGA, the exchange-correlation energy is written as a functional of the electron density and its gradient:

$$E_{xc}^{GGA}[\rho, \nabla\rho] = \int f(\rho, \nabla\rho) dq \quad (3.12)$$

The functional used for the calculations presented in Chapters 5 and 6 is the revised Perdew-Burke-Ernzerhof (RPBE) functional [5]. The quality of the RPBE functional and of several other functionals for gas phase reaction barrier heights is discussed in Refs. [6, 7].

3.3 Building the potential energy surface

To build the 6-dimensional (6D) potential energy surface for the $\text{H}_2 + \text{CO}/\text{Ru}(0001)$ system, we used the modified Shepard (MS) interpolation method implemented in the GROW-code [8–10] adapted for molecule-surface reactions [11]. (The potential is 6D because it depends on the six degrees of freedom of the H_2 molecule.) The surface atoms and the adsorbate (*i.e.* CO) are taken as frozen, after allowing the atoms to relax in the Z -direction. The fact that the reaction probability for hydrogen found in experiments for the clean Ru(0001) and for the CO/Ru(0001) system are independent of surface temperature [12, 13] suggests that this approximation is reasonable. Another approximation is the use of the Born-Oppenheimer approximation, neglecting electron-hole pair excitations (see Section 3.1).

3.3.1 Electronic structure calculations

The DFT calculations are done using the DACAPO code [14]. To describe the exchange-correlation energy of the electrons, the generalized gradient approximation (GGA) is used. Within this approximation the RPBE functional [5] is used. This functional is known to yield better chemisorption energies for CO on seven flat metal surfaces, including Ru(0001), than the PW91 functional [15]. For the dissociation of hydrogen on Ru(0001) both RPBE and

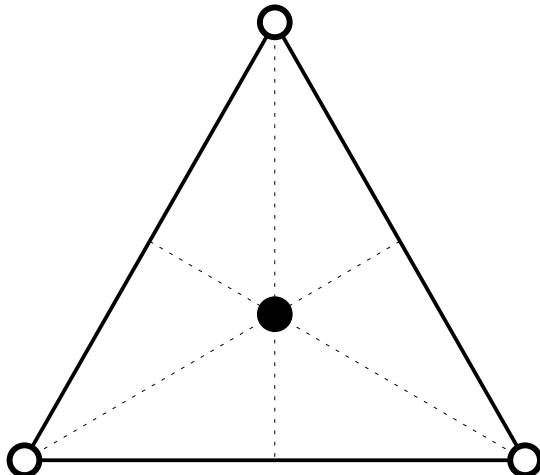


Figure 3.1: The equilateral triangle used for building the PES. The black atom is the Ru atom and the white atoms are the O atoms of the CO molecules.

PW91 do not yield chemical accuracy (43 meV) [12]. However, there is no systematic proof yet that other standard GGA functionals perform better for H_2 -metal surface reactions. We selected the RPBE functional because it better describes the CO-Ru interaction and because it describes dissociation of H_2 on bare Ru(0001) equally well as the PW91 functional. The ion cores are modeled using ultrasoft pseudo-potentials and a plane-wave basis set is used for the electronic orbitals.

3.3.2 Modified Shepard interpolation method

In the MS interpolation method, the interpolated PES is given by a weighted series of Taylor expansions centered on DFT data points, sampled throughout the configuration space of the system. Instead of the interatomic distances, the inverse interatomic distances, $Q_i = 1/R_i$, are used as coordinates. The vector defining any configuration of the system is given by $\mathbf{Q} = [1/R_1, \dots, 1/R_{n(n-1)/2}]$, where n is the number of atoms used to describe the system. We use six atoms to model the $\text{H}_2 + \text{CO}/\text{Ru}(0001)$ system: Two defining the H_2 molecule approaching the surface, and three O atoms of the CO molecule at the corners of the equilateral triangle, and one Ru atom describing the Ru atom in the middle of the triangle. Figure 3.1 shows a schematic picture of the atoms used. We also tested other coordinates representing the surface, but they gave either worse results, or similar results while consuming much more CPU-time.

For each configuration \mathbf{Q} , a set of $3n - 6$ algebraically independent linear combinations of the inverse interatomic distances can be defined as follows [9]:

$$\zeta_m = \sum_{k=1}^{n(n-1)/2} U_{mk} Q_k. \quad (3.13)$$

Here $m = 1, \dots, 3n - 6$, and U_{mk} is the transformation matrix from reciprocal to symmetrized

coordinates. The potential energy at any configuration \mathbf{Q} , near data point $\mathbf{Q}(i)$, can be expanded as a second-order Taylor expansion $T_i(\mathbf{Q})$, in the following coordinates

$$T_i(\mathbf{Q}) = V[\mathbf{Q}(i)] + \sum_{k=1}^{3n-6} [\zeta_k - \zeta_k(i)] \frac{\delta V}{\delta \zeta_k} \Big|_{\mathbf{Q}=\mathbf{Q}(i)} + \frac{1}{2} \sum_{k=1}^{3n-6} \sum_{j=1}^{3n-6} [\zeta_k - \zeta_k(i)] [\zeta_j - \zeta_j(i)] \frac{\delta^2 V}{\delta \zeta_k \delta \zeta_j} \Big|_{\mathbf{Q}=\mathbf{Q}(i)} + \dots \quad (3.14)$$

Here $V[\mathbf{Q}(i)]$, the value of the potential at $\mathbf{Q}(i)$, and the gradients at this point are calculated by DACAPO. The second derivatives are calculated using forward differencing of the gradients.

The total potential energy at any configuration is then taken as

$$V(\mathbf{Q}) = \sum_{g \in G} \sum_{i=1}^{N_{data}} w_{goi}(\mathbf{Q}) T_{goi}(\mathbf{Q}), \quad (3.15)$$

where $T_{goi}(\mathbf{Q})$ represents a second-order Taylor expansion, and $w_{goi}(\mathbf{Q})$ a normalized weight function (for more details see Refs. [9, 11]). N_{data} is the number of DFT data points in the interpolation, G is the symmetry group and goi is the transformation of the i th data point by the group element g . To take into account the full symmetry of the system, a sum is taken over both the DFT data points and their symmetry equivalent points.

In the MS interpolation the sampling of DFT data points is not uniformly distributed, in contrast to other interpolation methods (see *e.g.* Refs. [16, 17]). In the dynamically more important regions of the PES, a denser grid of data points is present. These regions are found performing classical trajectory calculations. The philosophy of the GROW method is that it is only necessary to know the PES in that region of space where the molecules are present during dynamics calculations. The new points are chosen according to one of the following criteria [8–10]: (i) The h-weight criterion, where it is assumed that the new point should be added in the region which the classical trajectories visit most frequently, unless (too) many data points are already present here. (ii) The variance criterion, where it is assumed that a new point should be added to the region in which the determination of the energy is the most inaccurate.

3.3.3 Implementation of the MS method in GROW

The appropriate data set is developed following an iterative scheme [8–10]:

- We start with an initial PES, which contains several data points located along different reaction paths. Those reaction paths are found by single point calculations varying r and Z for high symmetry sites, and by (adaptive) nudged elastic band calculations.
- Using such an initial PES 10 classical trajectory calculations are run. To ensure an accurate representation of the PES over the whole energy region possibly probed by a molecular beam for hydrogen molecules, we grow the PES simultaneously at different

kinetic energies and rovibrational quantum states. In the growth process we only consider H_2 molecules colliding at normal incidence.

- From the geometries obtained in step 2. a new point is chosen and added to the PES according to the criteria described in the above section.
- After updating the PES by adding the new point, the growth process is continued at step 2.
- After ~ 200 points are added to the PES the convergence is checked by computing the reaction and scattering probabilities from classical trajectory simulations using 5000 trajectories per initial set of conditions. When the reaction probability is converged, the growth process is stopped. In addition we plot 2D cuts and the density of points for the center-of-mass of the H_2 molecule in (X, Y) and (r, Z) .

3.4 Quantum dynamical calculations: the time-dependent wave packet method

The quantum dynamics calculations presented in Chapter 6 are obtained with the time-dependent wave packet (TDWP) method [18]. This method consists of three parts:

- setting up an initial wave packet
- propagating the initial wave packet in time
- asymptotic analysis of the wave packet.

TDWP calculations proceed as follows: An initial wave packet representing the molecule is placed far from the surface, so that the interaction between surface and molecule is negligible. Then the wave packet is propagated towards the surface. During this process, part of the wave function scatters back into the gas phase and part reacts at the surface. To obtain the scattering probabilities, the scattered part of the wave function is analyzed at regular time intervals at the asymptotic value of Z , where the molecule is considered to be in the gas phase. When the interaction of the scattered part of the wave packet is negligible, the propagation is stopped. Reaction and/or scattering probabilities are calculated.

In the TDWP method, the time-dependent Schrödinger equation is computed:

$$\hat{H}_{nuc}(\mathbf{R}, \mathbf{r})\Psi(t; \mathbf{R}, \mathbf{r}) = i\frac{\delta\Psi(t; \mathbf{R}, \mathbf{r})}{\delta t}. \quad (3.16)$$

For a time-independent Hamiltonian, $\hat{H}_{nuc}(\mathbf{R}, \mathbf{r})$, the formal solution of Eq. 3.16 is given by:

$$\Psi(t = \Delta t; \mathbf{R}, \mathbf{r}) = e^{-i\hat{H}_{nuc}(\mathbf{R}, \mathbf{r})\Delta t}\Psi(t = 0; \mathbf{R}, \mathbf{r}). \quad (3.17)$$

In Eq. 3.17, the exponential function is the time-evolution operator. It allows for the wave function to be written as a superposition of stationary scattering states, $\chi(E; \mathbf{R}, \mathbf{r})$:

$$\Psi(t = \Delta t; \mathbf{R}, \mathbf{r}) = \int_{-\infty}^{\infty} \chi(E; \mathbf{R}, \mathbf{r}) e^{-iE\Delta t} dE. \quad (3.18)$$

The stationary scattering state can also be written as a Fourier transform of the time-dependent wave function $\Psi(t; \mathbf{R}, \mathbf{r})$:

$$\chi(E; \mathbf{R}, \mathbf{r}) = \frac{1}{2\pi} \int_{-\infty}^{\infty} \Psi(t; \mathbf{R}, \mathbf{r}) e^{iEt} dt. \quad (3.19)$$

3.4.1 The initial wave packet

If the molecule is located far enough from the surface not to be influenced by it, *i.e.* if the molecule is located in the gas phase, its potential $V(\mathbf{R}, \mathbf{r})$ will be independent of \mathbf{R} :

$$\lim_{Z \rightarrow \infty} V(\mathbf{R}, \mathbf{r}) = V_{gas}(r), \quad (3.20)$$

and the potential can therefore be split into a gas phase potential V_{gas} , and an interaction potential V_{int} :

$$V(\mathbf{R}, \mathbf{r}) = V_{gas}(r) + V_{int}(\mathbf{R}, \mathbf{r}). \quad (3.21)$$

Using the limit of $Z \rightarrow \infty$ and Eq. 3.21 we can formulate $\hat{H}_{nuc}(\mathbf{R}, \mathbf{r})$ as:

$$\lim_{Z \rightarrow \infty} \hat{H}_{nuc}(\mathbf{R}, \mathbf{r}) = \hat{H}_{gas}(\mathbf{R}, \mathbf{r}) = \frac{-1}{2M} \nabla_{\mathbf{R}}^2 + \hat{K}_{vib}(r) + \hat{H}_{rot}(\mathbf{r}) + V_{gas}(r). \quad (3.22)$$

The eigen functions of $\hat{H}_{gas}(\mathbf{R}, \mathbf{r})$ can be taken as a direct product of a plane-wave function in \mathbf{R} and the molecule's nuclear eigen function corresponding to the rovibrational state κ , $\Phi_{\kappa}(\mathbf{r})$:

$$\hat{H}_{gas}(\mathbf{R}, \mathbf{r}) \{e^{i\mathbf{k}_0 \cdot \mathbf{R}} \cdot \Phi_{\kappa}(\mathbf{r})\} = (E_{kin}(\mathbf{k}_0) + E_{\kappa}) \cdot \{e^{i\mathbf{k}_0 \cdot \mathbf{R}} \cdot \Phi_{\kappa}(\mathbf{r})\}. \quad (3.23)$$

Here, $\mathbf{k}_0 = (k_0^X, k_0^Y, k_0^Z)$ is the momentum vector that describes the molecule's translational motion corresponding to its center-of-mass translational energy $E_{kin}(\mathbf{k}_0)$. E_{κ} corresponds to the rovibrational eigen energy for state κ . With Eq. 3.23, $\Psi(t = 0; \mathbf{R}, \mathbf{r})$ can now be taken as a linear superposition of plane-waves $e^{ik_0^Z Z}$ multiplied with a plane-wave function for initial parallel translational motion and the wave function describing the initial rovibrational state κ , $\Phi_{\kappa}(\mathbf{r})$:

$$\Psi(t = 0; \mathbf{R}, \mathbf{r}) = \Phi_{\kappa}(\mathbf{r}) \cdot e^{ik_0^X X + ik_0^Y Y} \cdot \int_{-\infty}^{\infty} b(k_0^Z) \cdot e^{ik_0^Z Z} dk_0^Z. \quad (3.24)$$

Here, $b(k_0^Z)$ can be taken to be a Gaussian shaped momentum distribution with average momentum \bar{k} and centered on $Z = Z_0$ with a half-width parameter σ :

$$b(k_0^Z) = \left(\frac{2\sigma^2}{\pi}\right)^{\frac{1}{4}} \cdot e^{-\sigma^2(\bar{k}-k_0^Z)^2} \cdot e^{i(\bar{k}-k_0^Z)Z_0}. \quad (3.25)$$

$b(k_0^Z)$ is a Gaussian wave packet corresponding to initial rovibrational state κ . If \bar{k} is negative and σ is sufficiently small, the wave packet describes molecules moving toward the surface with a range of translational energies.

3.4.2 Time propagation

In the calculations discussed in Chapter 6 the wave packet is propagated in time using the split operator (SPO) method [19]. In this method, the kinetic and potential part of the evolution operator (see Eq. 3.17) are separated:

$$e^{-i\hat{H}_{nuc}(\mathbf{R},\mathbf{r})\Delta t} = e^{-i\hat{K}\Delta t/2} \cdot e^{-i\hat{H}_{rot}\Delta t/2} \cdot e^{-i\hat{V}\Delta t} \cdot e^{-i\hat{H}_{rot}\Delta t/2} \cdot e^{-i\hat{K}\Delta t/2}. \quad (3.26)$$

where $\hat{K}(\mathbf{R},\mathbf{r}) = \frac{-1}{2M} \nabla_{\mathbf{K}}^2 + \hat{H}_{vib}(\mathbf{r})$. The error in the SPO method is due to the non-commutativity of the kinetic and potential energy operators. Due to the symmetric splitting, the errors are of order $O(\Delta t^3)$ [20, 21], instead of $O(\Delta t^2)$

$$\text{error} \approx \max \left[-i\frac{\Delta t^3}{8} [\hat{V}, [\hat{V}, \hat{K}]], -i\frac{\Delta t^3}{8} [\hat{K}, [\hat{K}, \hat{V}]] \right]. \quad (3.27)$$

By separating the kinetic and potential energy operators, we can evaluate the action of each on the wave function in its local representation. The wave function is transformed from coordinate to momentum space. The action of $e^{-i\hat{K}\Delta t/2}$ is merely multiplication by $e^{-i(k^2/(2m)\Delta t/2)}$. We then transform the wave function back to coordinate space, where the operator \hat{V} is local and evaluation of $e^{-i\hat{V}\Delta t}$ on the wave function is again a multiplication of two functions. This is repeated until the interaction of the scattered part of the wave packet is negligible.

An advantage of the split operator method is the simplicity of the implementation. A disadvantage is the relatively large error accumulation. To avoid this, fairly small time steps (1-5 atomic units) need to be used.

3.4.3 Asymptotic analysis of the wave packet

We extract information from the wave function during the propagation, to obtain reaction probabilities. This is done at a so-called asymptotic value of Z where interaction between the molecule and the surface is negligible. The part of the wave function that is analyzed, is no longer needed. An optical potential (see Section 3.4.4) is used to gradually absorb the wave function for $Z > Z_A$, where Z_A is the value of Z at which the wave function is analyzed.

The wave function is analyzed by a formalism originally developed by Balint-Kurti *et al.* for gas phase scattering [22–24], and which is adapted for molecule-surface scattering [25]. In this formalism, the scattered wave function is projected at $Z = Z_A$ onto the free particle states:

$$C_{nmv'j'm'_j}(Z_A, t) = \int \Psi(Z = Z_A, r, x, y, \theta, \varphi; t) \Phi_{nmv'j'm'_j}^*(r, x, y, \theta, \varphi) d\tau. \quad (3.28)$$

Here, $d\tau$ is an integration element and

$$\Phi_{nmvjm_j}(r, x, y, \theta, \varphi) = \varphi_{vj}(r) \frac{e^{i(\mathbf{K}^0 + \mathbf{G}_{nm}) \cdot \mathbf{L}}}{\sqrt{A}} Y_{jm_j}(\theta, \varphi). \quad (3.29)$$

In Eq. 3.29, $e^{i(\mathbf{K} + \mathbf{G}_{nm}) \cdot \mathbf{L} / \sqrt{A}}$ is a plane-wave translational wave function in x and y with diffraction quantum numbers n and m , normalized to the unit cell with area A .

After the propagation is completed, the time-dependent coefficients $C_{nmv'j'm'_j}(Z_A, t)$ are transformed to the energy domain by a Fourier transform:

$$A_{nmv'j'm'_j}(E) = \int_0^T e^{iEt} C_{nmv'j'm'_j}(Z_A, t) dt. \quad (3.30)$$

The probability for transition from the initial state with rotational quantum numbers (j_0, m_{j_0}) , vibrational quantum number v_0 and initial translational momenta k_Z , k_x , and k_y to the final state $(nmv'j'm'_j)$ is given by:

$$P = |S(nm, v', j', m'_j | v_0 j_0 m_{j_0}; k_x, k_y, -k_Z)|^2. \quad (3.31)$$

The S -matrix elements $S(nm, v', j', m'_j | v_0 j_0 m_{j_0}; k_x, k_y, -k_Z)$ are given by:

$$S(nm, v', j', m'_j | v_0 j_0 m_{j_0}; k_x, k_y, -k_Z) = \delta_{0n} \delta_{0m} \delta_{v_0 v'} \delta_{j_0 j'} \delta_{m_{j_0} m'_j} e^{-i2k_Z Z_A} - \left(\frac{k_Z k_{nmv'j'}}{2\pi} \right)^{\frac{1}{2}} \frac{e^{-ik_{nmv'j'} Z_A}}{Mb(-k_Z)} A_{nmv'j'm'_j}(E), \quad (3.32)$$

where

$$k_{nmvj} = [2M(E - \epsilon_{vj}) - (\mathbf{K} + \mathbf{G}_{nm})^2]^{1/2}. \quad (3.33)$$

In Eq. 3.33, ϵ_{vj} is the energy of the rovibrational state with quantum numbers v and j , $\mathbf{K} = (k_x, k_y)$ and $\mathbf{G}_{nm} = (n\Delta k_x, m\Delta k_y)$, where Δk_x and Δk_y are the diffraction quanta. The first term on the right-hand side of Eq. 3.32 involving the Kronecker delta functions cancels the contribution from the incident wave function to the time-integral in Eq. 3.30.

The reaction probability at energy E is then calculated by adding up all scattering probabilities and subtracting the sum from 1:

$$P_R(E) = 1 - \sum_{nmv'j'm'_j} |S(nm, v', j', m'_j | v_0 j_0 m_{j_0}; k_x, k_y, -k_Z)|^2. \quad (3.34)$$

3.4.4 Optical potential

The part of the wave function that has been analyzed, is no longer needed. It should be absorbed to avoid the storage of unnecessary data, and to avoid the use of very large grids in Z , necessary to be able to accommodate the wave function during propagation. The absorption of the wave function is achieved by using an imaginary potential defined between Z_{min} and Z_{max} outside the interaction region. By adding $V_{abs} = -iV_{opt}$, where V_{opt} is real, to the Hamiltonian in Eq. 3.17 a factor $e^{-V_{opt}}$ arises that will dampen the wave function if V_{opt} is taken as:

$$V_{opt} = \begin{cases} A_2 \left(\frac{Z - Z_{min}}{Z_{max} - Z_{min}} \right)^2 & \text{if } Z_{min} \leq Z \leq Z_{max} \\ 0 & \text{if } Z < Z_{min}, \end{cases} \quad (3.35)$$

where a good choice for Z_{min} is $Z_{min} = Z_A$. Here, V_{abs} is called an optical potential. Z_{max} is best taken as the last grid point in Z . The A_2 parameter should be chosen such that efficient absorption for all energies contained in the scattered wave packet will be achieved, while keeping the range over which the optical potential is defined minimal. The optical potential described in Eq. 3.35 is a quadratic potential, which absorbs efficiently for all energies contained in the wave packet.

An optical potential is also used to absorb the wave function in r . Once the internuclear distance r has exceeded some value r_d , we assume the molecule to be dissociated. So for values of $r > r_d$ the wave function is no longer needed. For absorption in r , also a quadratic optical potential is used.

3.4.5 Finite basis representations and discrete variable representations

In the time-dependent wave packet method, we repeatedly apply the Hamiltonian to the wave function, to propagate it in time. The way this application is performed, depends on the representation of the wave function. This representation therefore determines the efficiency of the TDWP method. The representations used in the calculations described in Chapter 6 are the finite basis representations (FBR) [26–29] and the discrete variable representations (DVR) [26–29], which are implementations of the collocation method [21].

In the basis set expansion method the wave function $\Psi(\mathbf{r})$ can be approximated by an expansion in a set of N linearly independent basis functions $f_n(\mathbf{r})$:

$$\Psi(\mathbf{r}) \approx \sum_{n=1}^N C_n f_n(\mathbf{r}). \quad (3.36)$$

In the collocation method, the N coefficients C_n of Eq. 3.36 are found by relating the wave function at N points in \mathbf{r} to the expansion and solving the N linear equations by a matrix inversion:

$$\Psi(\mathbf{r}_i) \equiv \Psi = \mathbf{fC}, \quad (3.37)$$

where $i = 1, \dots, N$. In Eq. 3.37, \mathbf{f} is an N -dimensional square matrix. It transforms the coefficient vector \mathbf{C} into the wave function vector Ψ . The inverse of the matrix \mathbf{f} , \mathbf{f}^{-1} , is used to obtain the vector \mathbf{C} from the vector Ψ by $\mathbf{C} = \mathbf{f}^{-1}\Psi$. Once we know \mathbf{C} , we approximate the action of a non-local operator in \mathbf{r} on $\Psi(\mathbf{r})$, $\widehat{O}(\mathbf{r})$ with $\widehat{O}(\mathbf{r})f_n(\mathbf{r}) = f'_n(\mathbf{r})$, by applying $\widehat{O}(\mathbf{r})$ to Eq. 3.36:

$$\widehat{O}(\mathbf{r})\Psi(\mathbf{r}) \approx \sum_{n=1}^N C_n \widehat{O}(\mathbf{r})f_n(\mathbf{r}) \approx \sum_{n=1}^N C_n f'_n(\mathbf{r}) \quad (3.38)$$

The advantage of the collocation method is the freedom of choice of $f_n(\mathbf{r})$ so that the computation of $\widehat{O}(\mathbf{r})f_n(\mathbf{r}) = f'_n(\mathbf{r})$ is easier than computing $\widehat{O}(\mathbf{r})\Psi(\mathbf{r})$ directly.

The matrix \mathbf{f}^{-1} effectively transforms the wave function at the N points \mathbf{r}_i into the N coefficients C_n . However, if the linearly independent basis functions $f_n(\mathbf{r})$ of Eq. 3.36 are chosen to be eigen functions of the operator $\widehat{O}(\mathbf{r})$ and are taken to be mutually orthogonal over the N discrete points \mathbf{r}_i :

$$\sum_{n=1}^N f_n^*(\mathbf{r}_k) f_m(\mathbf{r}_k) = \delta_{n,m}, \quad (3.39)$$

we can significantly simplify the collocation scheme. We do not have to invert the matrix \mathbf{f} because with Eq. 3.39 the following holds for Eq. 3.37:

$$\sum_{n=1}^N f_m^*(\mathbf{r}_k) \Psi(\mathbf{r}_k) = \sum_{n=1}^N \sum_{k=1}^N C_n f_n(\mathbf{r}_k) f_m^*(\mathbf{r}_k) = \sum_{n=1}^N C_n \delta_{n,m} = C_m. \quad (3.40)$$

If at the same time $\widehat{O}(\mathbf{r}_k) = o_n f_n(\mathbf{r}_k)$ holds, Eq. 3.38 reduces to:

$$\widehat{O}(\mathbf{r})\Psi(\mathbf{r}) \approx \sum_{n=1}^N C_n \widehat{O}(\mathbf{r})f_n(\mathbf{r}) \approx \sum_{n=1}^N C_n o_n f_n(\mathbf{r}) \approx \sum_{n=1}^N C'_n f_n(\mathbf{r}), \quad (3.41)$$

and the operator $\widehat{O}(\mathbf{r})$ is considered to be diagonal in the \mathbf{C} representation. We can now compute the effect of $\widehat{O}(\mathbf{r})$ on $\Psi(\mathbf{r})$ in three steps:

- Transformation of the DVR of $\Psi(\mathbf{r})$, Ψ , into the FBR of $\Psi(\mathbf{r})$, \mathbf{C} , by using $\mathbf{f}^{-1} = \mathbf{f}^\dagger$ because of Eq. 3.39.
- Application of the operator $\widehat{O}(\mathbf{r})$ on the FBR of $\Psi(\mathbf{r})$, to get \mathbf{C} , which is an FBR of $\widehat{O}(\mathbf{r})\Psi(\mathbf{r})$. The operator $\widehat{O}(\mathbf{r})$ can be represented as a diagonal matrix $\mathbf{O}_{nm} = \delta_{nm} o_n$ in the FBR, because only a vector-vector dot product is needed to apply $\widehat{O}(\mathbf{r})$ on \mathbf{C} .
- Transformation of \mathbf{C} , the FBR of $\widehat{O}(\mathbf{r})\Psi(\mathbf{r})$, back to the DVR of $\widehat{O}(\mathbf{r})\Psi(\mathbf{r})$, Ψ' by using \mathbf{f} .

We use the matrices \mathbf{f} and \mathbf{f}^{-1} to switch between the DVR and the FBR of the wave function. The two representations can be considered to be conjugate to each other [26–29]. Moreover, we can now express the complete procedure of applying $\widehat{O}(\mathbf{r})$ on $\Psi(\mathbf{r})$ in matrix vector notation as:

$$\Psi' = \mathbf{f} \mathbf{O} \mathbf{f}^{-1} \Psi \quad (3.42)$$

This method of applying an operator to a wave function is called pseudo-spectral (PS) because we make use of a discrete coordinate space and its conjugate space. In the calculations presented in Chapter 6 two different representations of the wave function based on the PS method are used.

Fourier representation of the wave function

The plane-wave functions have three properties. First, they are eigen functions of the Laplacian operator, $\nabla_r^2 e^{ik \cdot r} = -k^2 e^{ik \cdot r}$. Second, they are mutually orthogonal for a series of N equally spaced discrete points $r_n = nL/N$ over the range $[0, L]$:

$$\sum_{n=0}^{N-1} e^{\frac{-2\pi i p \cdot r_n}{L}} e^{\frac{-2\pi i q \cdot r_n}{L}} = N \delta_{p,q}, \quad (3.43)$$

where p and q are integers. Third, they form a complete set for periodic or band width limited functions of r [30]. According to Eq. 3.43, the discrete space conjugate to r_n , the momentum space, is given by $k_m = \frac{2\pi m}{L}$ with $0 \leq m \leq N-1$ so that $\Delta k = 2\pi/L$. The unitary change-of-basis matrix \mathbf{f} of Eq. 3.37 for plane-waves has the elements $\mathbf{f}_{mn} = e^{\frac{2\pi i m n}{N}}$. Plane-waves are often used to represent the wave function in translational or vibrational degrees of freedom, especially if there is periodicity associated with these degrees of freedom, because the plane-waves are eigen functions of the Laplacian operator and form a complete set for periodic functions. Transforms based on plane-waves are Fourier transforms and efficient algorithms are available to compute them. The Fast Fourier Transform (FFT) method scales approximately as $N \log N$ [31], whereas the normal, discrete Fourier transform scales as N^2 .

Gaussian quadratures

In order to obtain the discrete orthogonality of $f_n(\mathbf{r}_k)$ over the N points in \mathbf{r}_k in Eq. 3.39, we can also use continuous polynomials $p_n(\mathbf{r})$ mutually orthogonal with respect to a weighting function $\omega(\mathbf{r})$ over the range $[a, b]$:

$$\int_a^b \omega(\mathbf{r}) p_n^*(\mathbf{r}) p_m(\mathbf{r}) d\mathbf{r} = \delta_{n,m}. \quad (3.44)$$

In Eq. 3.44, assuming that $p_m(\mathbf{r})$ is an n^{th} order polynomial, $p_n^*(\mathbf{r}) p_m(\mathbf{r})$ is a polynomial of degree $n+m$ and the above orthogonality integral can be written as:

$$\int_a^b \omega(\mathbf{r}) P_{n+m}(\mathbf{r}) d\mathbf{r} = \delta_{n,m}. \quad (3.45)$$

According to the Gaussian quadrature theorem [26–30, 32, 33], the integral of Eq. 3.45 can be numerically calculated using the following formula:

$$\int_a^b \omega(\mathbf{r}) P_{n+m}(\mathbf{r}) d\mathbf{r} = \sum_{k=1}^N A_k P_{n+m}(r_k), \quad (3.46)$$

with

$$A_k = \int_a^b \frac{\omega(\mathbf{r}) p_N(\mathbf{r})}{(\mathbf{r} - \mathbf{r}_k) \cdot \left. \frac{\partial p_N(\mathbf{r})}{\partial \mathbf{r}} \right|_{\mathbf{r}=\mathbf{r}_k}} d\mathbf{r} \quad (3.47)$$

and r_k the N roots of the N^{th} order polynomial $p_N r$ which obeys Eq. 3.44. The numerical calculation of Eq. 3.46 is exact if $n + m \leq 2N - 1$. With these equations, Eq. 3.44 can be rewritten as

$$\delta_{n,m} = \int_a^b \omega(\mathbf{r}) p_n^*(\mathbf{r}) p_m(\mathbf{r}) d\mathbf{r} = \sum_{k=1}^N (\sqrt{A_k} p_n^*(\mathbf{r}_k)) (\sqrt{A_k} p_m(\mathbf{r}_k)) \quad (3.48)$$

and Eq. 3.39 can be obtained by setting $f_n(\mathbf{r}_k) = \sqrt{A_k} p_n(\mathbf{r}_k)$. With this choice, the transformation matrix \mathbf{f} of Eq. 3.37 will have the elements $\mathbf{f}_{kn} = \sqrt{A_k} p_n(\mathbf{r}_k)$ and can be shown to be an orthogonal matrix from Eq. 3.48 for real polynomials $p_n(\mathbf{r})$.

Gauss-Legendre representation

The plane-waves form a suitable basis set for degrees of freedom showing periodicity, or for evaluation of the action of operators as the Laplacian. However, the rotational kinetic energy operator of the Hamiltonian and the angular parts of the wave function require a different representation. The eigen functions of the rotational kinetic energy operator $\hat{H}_{rot}(\mathbf{r})$ of the Hamiltonian for a diatomic molecule, $\hat{H}_{rot}(\mathbf{r}) = \frac{\hat{j}^2}{2\mu r^2}$, are given by the spherical harmonics:

$$\frac{\hat{j}^2}{2\mu r^2} Y_{jm_j}(\theta, \varphi) = \frac{j(j+1)}{2\mu r^2} Y_{jm_j}(\theta, \varphi), \quad (3.49)$$

where μ is the reduced mass given by $\mu = \frac{m_1 m_2}{m_1 + m_2}$. A representation of the angular part of the wave function based on spherical harmonics would therefore be suitable. Moreover, because we can write the spherical harmonics as

$$Y_{jm_j}(\theta, \varphi) = \frac{1}{\sqrt{2\pi}} L_{m_j}^j(\cos\theta) \cdot e^{im_j\varphi} \quad (3.50)$$

with $L_{m_j}^j(x)$ being a normalized associated Legendre polynomial [29,30,33], an orthogonality relation for the $Y_{jm_j}(\theta, \varphi)$ exists:

$$\left\langle Y_{jm_j}(\theta, \varphi) | Y_{j'm'_j}(\theta, \varphi) \right\rangle = \delta_{j,j'} \delta_{m_j,m'_j}. \quad (3.51)$$

Because of Eq. 3.51, an orthogonal transform from the (j, m_j) FBR to the (θ, φ) DVR, based on Gaussian quadratures for θ and FFT's for φ can be formulated [29,32–35].

3.5 Quasi-classical trajectory calculations

To find the dynamically important regions during the 'growth' process carried out with the GROW code (see Section 3.3) and to calculate reaction probabilities, we perform quasi-classical trajectory (QCT) calculations. For these calculations we use the QCT method [36], in which the initial zero point energy (ZPE) of the hydrogen molecule is included in the dynamics by using an ensemble of initial conditions for the internal motion of the molecules that forms a classical microcanonical distribution. These kinds of calculations are susceptible to the so-called ZPE violation problem [37]. However, for an activated system such as H_2 dissociation on $\text{CO}/\text{Ru}(0001)$, this problem is expected to play a minor role at energies above the threshold to reaction. The QCT method is known to give accurate results for activated molecule-surface reactions [38–41]. In contrast to the CT method, vibrational softening (adiabatic transfer of energy from internal to translational motion) is taken into account. Not doing this may lead to underestimated reaction probabilities [40].

To compute the reaction probability of hydrogen we solve the classical equations of motion using the velocity-Verlet algorithm [42]. For each initial kinetic energy and initial rovibrational state, the probabilities are calculated as an average over the molecular initial conditions, *i.e.* internal coordinates and internal conjugated momenta. A Monte Carlo sampling method is used to simulate the molecular initial conditions for each set of initial parameters E_0, v_0 and j_0 . In order to obtain low statistical errors we compute 5000 trajectories for each value of E_i and rovibrational state of H_2 (D_2). We consider that dissociation has taken place when $r > 4a_0$ with a positive radial velocity. In contrast, we consider a molecule reflected when the molecular center-of-mass reaches its starting point in Z with the molecule's velocity vector pointing towards the vacuum.

To compute reaction probabilities as a function of m_j the initial angular momentum of the molecule is fixed using $L = \sqrt{j(j+1)}$. Its orientation is chosen randomly with the constraint:

$$\cos(\theta_L) = \frac{m_j}{\sqrt{j(j+1)}}, \quad (3.52)$$

where θ_L is the angle between L and the axis perpendicular to the surface.

3.6 Molecular beam simulation

In a supersonic molecular beam experiment the temperature of the nozzle determines the collision energy (with E_n ranging from 2.5 to $2.7T_n$) [43,44], the vibrational temperature

(equal to T_n) and the rotational temperature (equal to $0.8T_n$) of the impinging hydrogen molecules [43]. To compare our computed reaction probabilities to experiments done for the same system [13], we made a simulation of the molecular beam conditions used in the experiment, taking into account the energy (velocity) distribution in the beam and the vibrational and rotational states populated in the molecular beam for the different nozzle temperatures. The total reaction probability $R(T_n)$ that we compare to the measured reaction probability $S_0(E_n, T_n)$ (we use R for computed and S_0 for measured values) can be calculated from the fully energy resolved reaction probabilities $R(E_n; T_n)$ convoluted with the velocity distribution of the supersonic molecular beam by:

$$R(T_n) = \frac{\int_{v=0}^{v=\infty} f(v; T_n) R(E_n; T_n) dv}{\int_{v=0}^{v=\infty} f(v; T_n) dv}. \quad (3.53)$$

Here the flux weighted velocity distribution is given by [44, 45]:

$$f(v; T_n) = C v^3 e^{-\frac{(v-v_0)^2}{\alpha^2}} dv. \quad (3.54)$$

Here C is a constant, v is the velocity, T_n is the nozzle temperature, v_0 is the stream velocity and α is the width of the velocity distribution.

In Eq. 3.53 $R(E_n; T_n)$ is the energy-resolved reaction probability given by:

$$R(E_n; T_n) = \sum_{v,j} F_B(v, j, T_n) R(E_n; v, j), \quad (3.55)$$

where $R(E_n; v, j)$ is the energy resolved initial-state-selected reaction probability. The Boltzmann factor F_B is given by:

$$F_B(v, j, T_n) = e^{-E_{vib}(v)/kT_n} (2j+1) e^{-E_{rot}^v(j)/0.8kT_n} / N, \quad (3.56)$$

where N is a normalization factor given by:

$$N = \sum_{v,j} e^{-E_{vib}(v)/kT_n} (2j+1) e^{-E_{rot}^v(j)/0.8kT_n}, \quad (3.57)$$

and the rotational and vibrational energies are taken as [46]:

$$E_{vib}(v) = (v + \frac{1}{2})\omega_e - (v + \frac{1}{2})^2\omega_e x_e + (v + \frac{1}{2})^3\omega_e y_e. \quad (3.58)$$

$$E_{rot}^v(j) = B_e j(j+1) - \alpha_e (v + \frac{1}{2}) j(j+1). \quad (3.59)$$

The constants ω_e , $\omega_e x_e$, $\omega_e y_e$, B_e and α_e are taken from Ref. [46]. For calculation of the rotational and vibrational fractions used the presence of ortho and para hydrogen in the

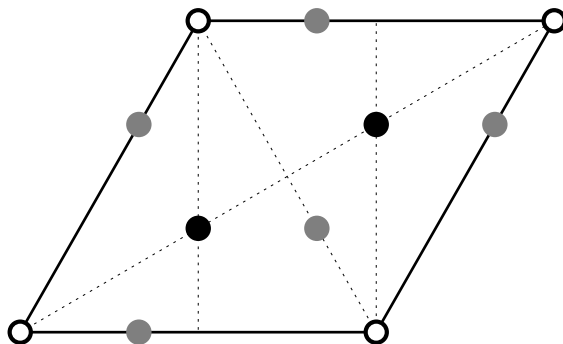


Figure 3.2: A schematic top view of the $(\sqrt{3} \times \sqrt{3})R30^\circ$ unit cell used to model the CO/Ru(0001) surface. The length of the unit cell is $\sqrt{3} * a = 4.75 \text{ \AA}$. The white circles represent O atoms (the only atoms of the CO molecule visible for perpendicular adsorption). The black and gray circles represent Ru atoms in the first (top) and second layers, respectively. Only the first and second Ru layers are shown.

molecular beam is taken into account (ortho= 75% for H_2 and 67% for D_2 , and para= 25% for H_2 and 33% for D_2) by multiplying the obtained fraction $F_B(v, J, m_J)$ with the appropriate fraction of ortho or para hydrogen.

To obtain the total computed reaction probability, quasi-classical trajectory calculations were done for a selection of relevant energies, and all relevant vibrational and rotational states. The 10-12 kinetic energy data points for all rovibrational states were interpolated using a cubic spline method. The energy distribution of the molecular beam was numerically integrated using points with equal spacing in the energy, and for each of these energies the reaction probability was taken from the cubic spline fit interpolation and its contribution to the total reaction probability was calculated.

3.7 The CO/Ru(0001) system

In a metal crystal, the atoms are arranged in a regular fashion. The Ru(0001) surface is flat, with a hexagonally closed packed (hcp) structure. In this structure the different layers have an ABA ordering, which means that the atoms in the third row are placed below the atoms in the first row. The atoms in the second row have different positions. The metal crystal consists of unit cells, which, when repeated in all directions, make up the entire crystal.

At the surface of the crystal, the same regularity is present, but in two dimensions. This regularity can be used to do the dynamics calculations using one unit cell, and then applying periodic boundary conditions. The smaller the unit cell chosen, the less computational time is needed for the calculations. The smallest possible unit cell for the Ru(0001) surface, is the 1x1 unit cell. When adding CO to the Ru(0001) surface, the unit cell changes. Here we study the ruthenium system with 1/3 monolayer (ML) of CO adsorbed. It is experimentally observed by LEED that this corresponds to a $(\sqrt{3} \times \sqrt{3})R30^\circ$ structure [47–50]. A picture of the corresponding unit cell is given in Fig. 3.2. For the Ru slab the nearest neighbor distance a used in the calculations corresponds to 2.745 \AA , compared to an experimental value of 2.71 \AA and a relaxed interlayer distance c of $\sim 2.12 \text{ \AA}$, compared to an experimental

value of 2.14 \AA , is used. The sides of the CO/Ru(0001) unit cell thus have a length of $2.745 * \sqrt{3} \text{ \AA}$. The skewing angle is 60° .

References

- [1] M. Born and R. Oppenheimer, *Annalen der Physik* **389**, 457 (1927).
- [2] P. Nieto, E. Pijper, D. Barredo, G. Laurent, R. A. Olsen, E. J. Baerends, G. J. Kroes, and D. Farías, *Science* **312**, 86 (2006).
- [3] P. Hohenberg and W. Kohn, *Phys. Rev. B* **136**, B864 (1964).
- [4] W. Kohn and L. J. Sham, *Phys. Rev. A* **140**, 1133 (1965).
- [5] B. Hammer, L. B. Hansen, and J. K. Nørskov, *Phys. Rev. B* **59**, 7413 (1999).
- [6] C. Y. Zhao and D. G. Truhlar, *J. Chem. Phys.* **128**, 184109 (2008).
- [7] J. Zheng, C. Y. Zhao, and D. G. Truhlar, *J. Chem. Theor. Comp.* **5**, 808 (2009).
- [8] M. J. T. Jordan, K. C. Thompson, and M. A. Collins, *J. Chem. Phys.* **102**, 5647 (1995).
- [9] K. C. Thompson, M. J. T. Jordan, and M. A. Collins, *J. Chem. Phys.* **108**, 8302 (1998).
- [10] R. P. A. Bettens and M. A. Collins, *J. Chem. Phys.* **111**, 816 (1999).
- [11] C. Crespos, M. A. Collins, E. Pijper, and G. J. Kroes, *J. Chem. Phys.* **120**, 2392 (2004).
- [12] I. M. N. Groot, H. Ueta, M. J. T. C. van der Niet, A. W. Kleyn, and L. B. F. Juurlink, *J. Chem. Phys.* **127**, 244701 (2007).
- [13] H. Ueta, I. M. N. Groot, M. A. Gleeson, S. Stolte, G. C. McBane, L. B. F. Juurlink, and A. W. Kleyn, *Chem. Phys. Chem.* **9**, 2372 (2008).
- [14] DACAPO, <http://www.camp.dtu.dk/campos/Dacapo/>.
- [15] E. Christoffersen, P. Stoltze, and J. K. Nørskov, *Surf. Sci.* **505**, 200 (2002).
- [16] H. F. Busnengo, A. Salin, and W. Dong, *J. Chem. Phys.* **112**, 7641 (2000).
- [17] R. A. Olsen, H. F. Busnengo, A. Salin, M. F. Somers, G. J. Kroes, and E. J. Baerends, *J. Chem. Phys.* **116**, 3841 (2002).
- [18] E. Pijper, G. J. Kroes, R. A. Olsen, and E. J. Baerends, *J. Chem. Phys.* **117**, 5885 (2002).
- [19] M. D. Feit, J. A. Fleck, and A. Steiger, *J. Comput. Phys.* **47**, 412 (1982).
- [20] L. L. Halcomb and D. J. Diestler, *J. Chem. Phys.* **84**, 3130 (1986).
- [21] R. Kosloff, *J. Phys. Chem.* **92**, 2087 (1988).

- [22] G. G. Balint-Kurti, R. N. Dixon, and C. C. Marston, *J. Chem. Soc., Faraday Trans.* **86**, 1741 (1990).
- [23] C. C. Marston, G. G. Balint-Kurti, and R. N. Dixon, *Theor. Chim. Acta* **79**, 313 (1991).
- [24] G. G. Balint-Kurti, R. N. Dixon, and C. C. Marston, *Int. Rev. Phys. Chem.* **11**, 317 (1992).
- [25] R. C. Mowrey and G. J. Kroes, *J. Chem. Phys.* **103**, 1216 (1995).
- [26] A. S. Dickinson and P. R. Certain, *J. Chem. Phys.* **49**, 4209 (1968).
- [27] J. V. Lill, G. A. Parker, and J. C. Light, *Chem. Phys. Lett.* **89**, 483 (1982).
- [28] J. P. Hamilton and J. C. Light, *J. Chem. Phys.* **84**, 306 (1986).
- [29] G. C. Corey, J. W. Tromp, and D. Lemoine, in *Numerical grid methods and their applications to the Schrödinger equation*, edited by C. Cerjan (Kluwer Academic, Dordrecht, 1993), volume 412, pp. 1–23.
- [30] G. B. Arfken and H. J. Weber, *Mathematical methods for physicists* (Academic Press, San Diego, 1995).
- [31] A. Besprozvannaya and D. J. Tannor, *Comput. Phys. Commun.* **63**, 569 (1991).
- [32] D. Lemoine and G. C. Corey, *J. Chem. Phys.* **92**, 6175 (1990).
- [33] G. C. Corey and D. Lemoine, *J. Chem. Phys.* **97**, 4115 (1992).
- [34] D. Lemoine and G. C. Corey, *J. Chem. Phys.* **94**, 767 (1991).
- [35] D. Lemoine, *Comput. Phys. Commun.* **97**, 331 (1996).
- [36] M. Karplus, R. N. Porter, and R. D. Sharma, *J. Chem. Phys.* **43**, 3259 (1965).
- [37] Y. Guo, D. L. Thompson, and T. D. Sewell, *J. Chem. Phys.* **104**, 576 (1996).
- [38] D. A. McCormack and G. J. Kroes, *Phys. Chem. Chem. Phys.* **1**, 1359 (1999).
- [39] D. A. McCormack, G. J. Kroes, R. A. Olsen, J. A. Groeneveld, J. N. P. van Stralen, E. J. Baerends, and R. C. Mowrey, *Faraday Discuss.* **117**, 109 (2000).
- [40] E. Pijper, M. F. Somers, G. J. Kroes, R. A. Olsen, E. J. Baerends, H. F. Busnengo, A. Salin, and D. Lemoine, *Chem. Phys. Lett.* **347**, 277 (2001).
- [41] P. Riviere, H. F. Busnengo, and F. Martín, *J. Chem. Phys.* **123**, 074705 (2005).
- [42] W. C. Swope, H. C. Andersen, P. H. Berens, and K. R. Wilson, *J. Chem. Phys.* **76**, 637 (1982).
- [43] K. D. Rendulic, G. Anger, and A. Winkler, *Surf. Sci.* **208**, 404 (1989).
- [44] C. T. Rettner, H. A. Michelsen, and D. A. Auerbach, *J. Chem. Phys.* **102**, 4625 (1995).

- [45] D. J. Auerbach, in *Atomic and molecular beam methods, vol. I*, edited by G. Scoles (Oxford University Press, 1988), pp. 362–379.
- [46] G. Herzberg, *Molecular spectra and molecular structure I. Spectra of diatomic molecules* (D. van Nostrand Company, Inc., Princeton, 1950).
- [47] E. D. Williams and W. Weinberg, *Surf. Sci.* **82**, 93 (1979).
- [48] H. Pfnür, D. Menzel, F. M. Hoffmann, A. Ortega, and A. M. Bradshaw, *Surf. Sci.* **93**, 431 (1980).
- [49] G. Michalk, W. Moritz, H. Pfnür, and D. Menzel, *Surf. Sci.* **129**, 92 (1983).
- [50] H. Pfnür and D. Menzel, *Surf. Sci.* **148**, 411 (1984).

